,

Optimal occlusion uniformly partitions red blood cells fluxes within a microvascular network

Shyr-Shea Chang,[1] Shenyinying Tu,[1] Yu-Hsiu Liu,[2] Van Savage,[3] Sheng-Ping L. Hwang,[4] and Marcus Roper[1]

[1] *Dept. of Mathematics, University of California Los Angeles, Los Angeles, CA 90095, USA*

[2] *Institute of Zoology, National Taiwan University, Taipei, Taiwan 10617, R.O.C.*

[3] *Dept. of Biomathematics, University of California Los Angeles, Los Angeles, CA 90095, USA*

[4] *Institute of Cellular and Organismic Biology, Academia Sinica, Nankang, Taipei, Taiwan 115, R.O.C.*

arXiv:1512.04184v2 [q-bio.TO] 23 Nov 2016

In animals, gas exchange between blood and tissues occurs in narrow vessels, whose diameter is typically less than that of a red blood cell. Red blood cells must deform to squeeze through these narrow vessels transiently blocking or occluding the vessels they pass through. Although the dynamics of vessel occlusion have been studied extensively, it remains an open question why microvessels need to be so narrow. We study occlusive dynamics within a model microvascular network: the embryonic zebrafish trunk. We show that pressure feedbacks created when red blood cells enter the finest vessels of the trunk act together to uniformly partition red blood cells through the microvasculature. Using models as well as direct observation, we show that these occlusive feedbacks are tuned throughout the trunk network to prevent the vessels closest to the heart from short-circuiting the network. Thus occlusion is linked with another open question of microvascular function: how are red blood cells delivered at the same rate to each micro-vessel? Our analysis shows that tuning of occlusive feedbacks increase the total dissipation within the network by a factor of 11, showing that uniformity of flows rather than minimization of transport costs may be prioritized by the microvascular network.

I. INTRODUCTION

Vascular networks transport oxygen, carbon dioxide and sugars within animals. Exchange of both nutrients and gases occurs primarily in narrow vessels that are typically organized into reticulated networks. The narrowest vessels are often smaller even than red blood cells, forcing cells to squeeze through the vessels. Accordingly, hereditary disorders or diseases affecting the elasticity of cells and that prevent them from contorting through narrow vessels can disrupt microvascular circulation [1]. The rate at which energy must be expended to maintain a constant flow of blood through a vessel increases with its radius raised to the power of minus 4. The cost of blood flow transport in the cardiovascular system is thought to dominate the metabolic burden on animals [2], and capillaries and arterioles account for half of the total pressure drop within the network, and thus half of its total dissipation [3]. Since red blood cells occlude the vessels that they pass through, even higher energy investments is required to maintain red blood cell movements in narrow vessels [4]. Indeed red blood cell deformation requires chemical power: experiments in which cells are deformed using optical tweezers, or by being pushed through synthetic channels with diameters comparable to real capillaries have shown that the extreme deformability of mammalian red blood cells requires continous ATP powered-remodeling of the connections between membrane and cytoskeleton [5, 6]. ATP released by deformed cells may induce vasodilation facilitating passage of cells through the narrowest vessels [7].

Why do micro-vessels need to be so narrow? A textbook answer to this question is that smaller, more numerous capillaries allow for more uniform vascularization of tissues – ensuring that "no cell is ever very far from a capillary" [3]. If smaller vessels are favored physiologically and red blood cell diameter acts as a lower bound on capillary diameters, then networks in which capillary diameters match those of red blood cells may be selected for. However, red blood cell sizes do not seem to be stiffly constrained – for example measured red blood cell volumes vary over almost an order of magnitude (19 to 160 femto-liters) between different mammals [8]. Since for a fixed capillary diameter, a small decrease in red blood cell diameter would greatly reduce rates of energy dissipation for red blood cells traveling through capillary beds [9], the evolutionary forces maintaining red blood cells and capillary diameters remain unclear. There is a natural analogy between occlusion of vessels by cells, and the congestion that occurs in data or road networks [10]. Efforts to construct efficient transport networks often focus on reducing congestion [10]. Previous work has shown that the deformation of cells passing through capillaries may be an adaptive feature of the cardiovascular network. By directly stretching cells using optical tweezers Rao et al. [11] showed that deforming red blood cells releases oxygen. But it remains an untested hypothesis that squeezing cells so that they may pass through capillaries accelerates oxygen release, and therefore contributes to the function of the cardiovascular network. Indeed,

earlier models suggest that alterations in the shape of the red blood cell surface decrease rates of oxygen exchange [12].

In this work we develop and test a previously unreported contribution of occlusive dynamics to the efficient functioning of the cardiovascular network. Specifically we tie occlusive dynamics to a different open mystery of cardiovascular function – given that microvessels are distributed throughout the body and at very different distances from the heart, there is surprising consistency among measured flow-rates in different capillaries [13–15]. Indeed consistency in flow rates may be chemically necessary: if flow rate in a capillary is too low, the cells surrounding the capillary may not receive enough oxygen, but if the flow rate is too high, then red blood cells may leave the capillary bed before surrendering their oxygen to the surrounding cells. If the cardiovascular system is treated as an idealized symmetric branching network (such as in [2]) then flows are automatically uniformly partitioned at each level of the network, including among capillaries. But real cardiovascular networks have complex topologies, and it is not clear how the uniform flow can be achieved among billions of capillaries whose distances from the heart can range over several orders of magnitude.

In this work we show that in the embryonic zebrafish, a model system for studying cardiovascular development [16], these two questions may be closed linked. Tuned occlusion – i.e. small differences in the resistance that vessels present to cells – ensures that red blood cells are uniformly partitioned between the finest vessels within the zebrafish trunk. Our experimental observations confirm previous measurements that red blood cells are uniformly partitioned between fine vessels [15], yet in the absence of tuned occlusion, we demonstrate that the vessels closest to the zebrafish heart would receive 11-fold higher rates of flow that vessels furthest from the heart. In other words these vessels would act as hydraulic short-circuits. In further support of the hypothesis that occlusion is an adaptive feature of the network we calculate optimal occlusive dynamics – i.e. the distribution of occlusive feedbacks that leads to the most uniform partitioning of red blood cells between the smallest vessels. The occlusive feedbacks within the real zebrafish conform very closely to this optimal distribution.

Microvascular networks have been postulated to be organized to minimize the hydraulic costs of blood transport [17–19]. Certainly in larger vessels within both the arterial and venous vascular network, vessel radii appear to be organized to minimize hydrodynamic dissipation [20, 21]. Yet, our results suggest that rather than eliminating cellular congestion fine vessels make use of it. As a direct demonstration of the tradeoffs between minimizing the cost of transport and tuning occlusion to route red blood cells uniformly, we show that the optimal distribution of occlusive feedbacks increases hydraulic dissipation in the network 11 fold compared with a network in which the

smallest measured occlusive feedbacks occur within each vessel. Thus, taken together, our results advance an potential new optimization principle – uniform routing of red blood cells – that may underlie the organization of microvascular networks generally.

II. MATERIAL AND METHODS

A. Imaging zebrafish trunk vessels and red blood cell movements

To experimentally measure the flow and the geometry of zebrafish trunk network we analyzed confocal images of a 4 day post fertilization (dpf) transgenic Tg(gata1:dsRed; fli1a:EGFP) zebrafish that was anesthetized in 0.016% tricaine and embeded in 1% low gelling temperature agarose on a microscope slide. In this transgenic fish line, fli1a, a transcription factor associated with blood vessel morphogenesis is tagged with green fluorescent protein, causing the endothelial cells surrounding blood vessels to fluoresce green. Additionally, GATA-1, a transcription factor associated with erythrogenesis is tagged with red fluorescent protein, so that the red blood cells traveling through the GFP-labelled network fluoresce red. We measured vessel lengths and radii from GFP-images (showing the endothelial layers) taken under 10× magnification using a Zyla sCMOS camera on a Zeiss Axio Imager A2 fluorescent microscope were measured. To measure the flows, the same scope was used to take images in the DsRed channel at time intervals of $0.078 - 0.107$ sec. Red blood cells were manually tracked in image sequences using ImageJ [22].

B. Mathematical modeling of occlusion and parameter estimation

Flow is laminar within each zebrafish microvessel[23, 24]. The Womersley number [25], which for a vessel of diameter d, carrying blood with kinematic viscosity ν, and with heart rate f, is given by $Wo = \frac{2\pi f d^2}{\nu}$, measures the relative sizes of blood acceleration to viscous stresses. Within the largest trunk vessels $d \approx 12\,\mu$m, the viscosity of whole blood is $\nu \approx 5 \times 10^{-6}$ m^2/s [26], and the heart-rate is approximately $f = 2$ s^{-1}, so $Wo = 3.6 \times 10^{-4} \ll 1$, meaning that we may neglect pulsatile effects. Flow is uniform along each vessel, except within an entry region whose length is $\ell \sim Ud^2/\nu$ for a vessel of diameter d, through which blood travels at a speed U [27]. Maximum blood velocities on the order of 0.3 cm/s [28], so using the diameter of the largest trunk vessels we obtain: $\ell \approx 0.3\,\mu$m. Since the entry region is much smaller than the typical vessel length, we treat the flow in each vessel as being uniform along its length. Putting these ingredients together, we find that the flow through each vessel is inversely proportional to the resistance of the vessel, and the resistance may be calculated using Stokes' equations from the geometry of the vessel

and from the number of red blood cells that it contains. Mechanistic models to predict the motions of red blood cells through micro-vessels or through microfluidic channels with comparable diameters have been developed in previous works [4, 28, 29]. Throughout this work we adopt a model for red blood cell occlusion, in which the resistance of each vessel increases linearly with the number of red blood cells present. That is, if the number of red blood cells in a narrow vessel is given by n, then its resistance is given by an equation:

$$R(n) = R_0 + n\alpha_c \ . \tag{1}$$

where R_0 is the resistance of the vessel in the absence of red blood cells, i.e. is given by the Hagen-Poiseuille law, so that for a vessel of length ℓ and radius r: $R_0 = \frac{8\mu_{pl}\ell}{\pi r^4}$, where $\mu_{pl} \approx 1cP$ is the viscosity of the non-red blood cell component of the flood. Here the parameter α_c, which we call the occlusion strength in this paper, gives the increase in vessel resistance per red blood cell. Equation (1) represents a form of the Fahraeus-Lindqvist effect, which states that the apparent viscosity of blood, i.e. $R(n)\pi r^4/8\mu_{pl}\ell$, increases with hematocrit, i.e. with the concentration of red blood cells. The Fahraeus-Lindqvist effect also states that, for sufficiently narrow vessels, the apparent viscosity of blood also increases as vessel radius decreases: which can be captured in our model if the resistance per cell, α_c, increases. Equation (1) can be derived from the micromechanical model of [30]. Indeed any model in which the pressure drop across the red blood cell is proportional to the velocity of the cell will produce a relationship like Equation (1), and so identical equations are also used to model the traffic of droplets or particles through microfluidic channels [31]. In all of these models, α_c depends on the specific details of how the movements of cells, droplets or particles along the walls of the capillary or channel are lubricated. α_c therefore depends on parameters that we can not measure experimentally, including the thickness and porosity of the polymeric brush, or glyocalyx, that coats the endothelial wall of the capillary, as well as being sensitive to changes in vessel radius [29] that are too small to be detected in light microscopy. Accordingly we treat α_c as a phenomenological constant, to be measured directly by fitting Equation (1) to real flow data. Specifically for each micro-vessel, we can measure both the velocity of flow within the vessel and the number of red blood cells that it contains. The pressure difference across each vessel varies in time due to the variable pressure within the aorta, and also, less predictably because since the resistance of all vessels changes from moment to moment, there are pressure feedbacks across the entire network. But we assume that there is an overall average pressure drop across each vessel. Under conditions of constant pressure drop, the velocity of cell movement, v, in each vessel will be inversely proportion to the vessel resistance $R(n)$. Thus Equation (1) predicts that a plot of $1/v$ against n will give a straight line, the slope of which can be used to calculate α_c. Here we used the modeled flows in the fine vessels where no red blood cell is present to determine the intercepts, which can be calculated by

using Hagen-Poiseuille formula (see Section III B). By regressing $1/v$ against n for each micro-vessel we calculate the variation of occlusive effects through the network (see Supplementary Materials for more details of the regression).

C. Incorporating occlusion into transport models

To study how varying occlusive effects between different microvessels may affect distribution of red blood cells, we incorporated Equation (1) into both continuum and discrete models of transport through the network.

For continuum level modeling, we assumed that the concentration of red blood cells was a constant, ρ, in each vessel. *Skimming* of red blood cells can occur when flows divide at vessel junctions – that is red blood cells may split in different proportions than whole blood [32] – but skimming was not seen in our data, and can not account for the uniformity of red blood cell flows, as we discuss in the results section. Thus if the constant concentration (#/volume) of red blood cells is ρ, then a vessel of volume V is expected to contain $n = \rho V$ cells. Once each vessel in the network has been assigned a resistance, then we can solve for the flows in the entire network, by applying Kirchoff's first law (conservation of flux) to calculate the pressure at each branching and fusion point, and then using the pressure difference across each vessel to calculate flows [18, 33, 34]. We discuss the geometry of the network and boundary conditions in the Results section.

Since each micro-vessel is so small, typically each vessel contains no more than one or two cells at a time. For this reason we expected Poisson noise effects (i.e. fluctuations in the number of cells contained within each vessel) to influence red blood cell fluxes. We therefore built a discrete model, in which the trajectories of every single red blood cell traveling through the trunk network were directly simulated. Our discrete model is based on the droplet traffic model of [31]. Initially 990 cells are distributed uniformly through aorta according to measured zebrafish red blood cell concentrations [35]. At each step we calculate the resistance for each capillary by Eqn (1), and then use the hydraulic resistor network model to calculate the whole blood flow rates within each vessel. We then let cells travel according to the predicted whole blood velocity in their vessel. When a cell arrives at a node of the network; i.e. at a point where a vessel branches into two, which vessel it enters is determined randomly by a Bernoulli process with probability determined by the flow rate ratio of the two vessels. Flows are then recomputed for the new distribution of cells. Cells that leave the network, i.e. reach the end of one of the vessels within the simulated part of the network are immediately reintroduced into the network via the aorta. For each combination of parameters, we simulated 1000 s of red blood cell movement, with a time step of 0.1 s. The total inflow into the trunk via the aorta was set to fit the mean flux across all fine vessels to the experimentally measured mean flux.

III. RESULTS

A. Geometry of the zebrafish trunk microvasculature

The 4 day post fertilization zebrafish trunk vasculature is topologically simple. Oxygenated red blood cells (henceforth RBCs) flow into the zebrafish trunk via the dorsal aorta (DA) and return the heart via the posterior cardinal vein (PCV). The microvasculature consists of a series of parallel intersegmental vessels (Se) that, if the vasculature were laid flat, would span between the aorta and cardinal vein like the rungs of a ladder (Fig. 1A). Se are divided into intersegmental arteries (SeA) that connect to the aorta, and intersegmental veins (SeV) that connect to the posterior cardinal vein. SeA and SeV connect via another vessel called the Dorsal Longitudinal Anastomotic Vessel (DLAV), and in different parts of the DLAV, red blood cells flow toward the tail of the fish or toward its head. Red blood cells can enter the PCV by flowing along one of the SeA, through a section of the DLAV, and then along one of the SeV. Significantly, however, they can also flow directly from the DA into the PCV, since the two connect at the far end of both vessels in the tail of the fish.

In our simulations and modeling we simplified the network even further by assuming symmetry along the DLAV. Thus we ignored the PCV, DLAV and SeV, and simply modeled flows in the DA and SeA. To capture the symmetry of the network, we applied the same pressure boundary condition at the ends of each SeA and at the point where the DA fuses with the PCV, while maintaining flow into the network through the DA. Since only differences in pressure are needed to create flows within the network, we may without loss of generality set the pressure at the ends of each SeA to be equal to 0; i.e. use the DLAV as a pressure reference.

B. Absence of occlusion produces uneven fluxes within the Se

As a first step we calculated the RBC flux in intersegmental arteries (SeA) with no occlusion or untuned occlusive effects and compared to experimental measurements. That is we approximated the resistance of each vessel using (1) with $\alpha_c = 0$ and treating the blood as a continuous phase, so that μ_{pl} replaced by μ_{wb}, the viscosity of whole blood ($\mu_{wb} \approx 5$ cP in zebrafish [26]). We measured the lengths of each vessel directly from fli1a-EGFP images. SeAs were all assigned the same radius (2.9 μm), while because the DA tapers from the head to the tail, we independently measured DA radii between each SeA (see Supplementary Materials). We focus on the arterial network made up of SeA and DA vessels. We identify the vertices in this network, i.e. the points at which vessel branch of fuse, as points $i = 1, 2, \ldots n$, with respective pressures p_i (Fig. 1B). The number of SeAs, n, increases as the fish grows: for the 4

dpf zebrafish in our experiments $n = 12$. If vertices i and j are connected by a vessel, with resistance R_{ij}, then the total flow of blood along this vessel will be $(p_i - p_j)/R_{ij}$. Solving for the flows in the network is equivalent to finding the pressures $\{p_i\}$. For the zebrafish cardiovascular network we labeled vertices along the DA as $i = 1, 2, \ldots, n$. A vertex, $i = n+1$, represents the end of the DA in the tail of the zebrafish, where it connects directly to the PCV, and we label the vertices where the SeA meets the DLAV as $i = n+2, n+3, \ldots 2n+1$, . At vertices $i = n+1, \ldots 2n+1$, our symmetry boundary conditions require that $p_i = 0$. Thus only the pressures $\{p_i : i = 1, \ldots n\}$ need to be determined. We find these pressures by applying Kirchoff's First Law (conservation of flux), at each point where the pressure is determined, i.e. $\sum_{j \in n(i)} (p_i - p_j)/R_{ij} = 0$, except at $i = 1$ (the vertex closest to the heart). At this vertex, $\sum_{j \in n(1)} (p_1 - p_j)/R_{1j} = F$, where F is the total supply of blood to the trunk. All summations are taken over the neighbor set, $n(i)$, i.e. over all vertices that are linked to i. Although in principle, the flow F, can be measured directly from the flow in the DA as it joins the trunk network, we found these flows, difficult to measure in practice, since red blood cells travel so quickly in the DA that their tracking requires specialized microscopy methods [28, 36]. Instead in this analysis, and in all others, we used F as a free parameter to fit our models to experimental data.

The model of the zebrafish trunk microvasculature as an hydraulic resistor network follows many previous capillary network models (see e.g. [18, 33, 34]). The equations are formally identical to those for an electrical resistor network, with pressures replacing voltages, and flow rates replacing currents. Just as placing a wire across the terminals of a battery in an electrical resistor network will short circuit the network (i.e. divert current from higher resistance paths), the first SeA is predicted to receive the majority of the blood flow from the zebrafish trunk, with flow rates decreasing exponentially rapidly with distance from the heart. In total there is a predicted 11-fold difference between the flows through the first and last vessels (Fig. 1C).

An approximate model that treats each SeA has having the same resistance, and assigns same resistances to each segment of DA between SeAs (i.e. ignores DA taper) quantitatively reproduces the exponential decay. To build the approximate model we assume that each segment of the DA has the same hydraulic resistance, and that each SeA has the same resistance. Using the measured mean radii and lengths, each DA has the same conductance, written as: $\kappa_1 = 1/R_1 = 9.4 \times 10^5$ μm^{4}s/g, while all Se vessels have the same conductance, written as: $\kappa_2 = 1/R_2 = 3.9 \times 10^4$ μm^{4}s/g. Then conservation of flow at vertex $i = 2, \ldots, n$ gives:

$$-\kappa_1 p_{i-1} + (2\kappa_1 + \kappa_2) p_i - \kappa_1 p_{i+1} = 0 \ , \tag{2}$$

This is a second order recursion relation with constant coefficients. Its general solution is:

$$p_i = C_+ \xi_+^i + C_- \xi_-^i , \tag{3}$$

where $\xi_\pm$ are the roots of the auxiliary polynomial $\xi^2 - (2+\lambda)\xi + 1 = 0$, in which there is a single dimensionless parameter: $\lambda = \frac{\kappa_2}{\kappa_1} = 0.04$. This equation has two roots, with $\xi_+ > 1$ and $\xi_- < 1$. In general C_+ and C_- must both be non-zero to satisfy our boundary conditions (namely $p_{n+1} = 0$ and $F = \kappa_2 p_1 + \kappa_1(p_1 - p_2)$). However the two components give rise to exponentially growing and decaying pressures respectively. Typically the first term will negligible, except potentially in a small boundary layer region consisting of the vertices in the tail. Therefore over most vertices $p_i \sim C_- \xi_-^i$, i.e. the pressure decays exponentially with distance from the heart, as must flows in the SeAs. For the real zebrafish network: $\xi_- = 0.81$. Despite the simplification in geometry, the analytic formula agrees quite well with the solution to the full system of linear equations (compare gray and black curves in Fig. 1C). Additionally, for any $\lambda > 0$, it is impossible to organize an auxiliary polynomial without one having one root $\xi_- < 1$, so exponential decay in fluxes is an inescapable feature of the ladder-like geometry of the trunk vasculature.

Although embryonic tissues receive oxygen primarily by diffusion through the skin [37, 38], vascular transport of oxygen becomes essential to embryo development after 2.5 weeks[39]. So we expect that a zebrafish with such large differences in fluxes between trunk vessels would be disadvantaged. Because oxygen can diffuse through the zebrafish tissues, we first verified that the differences in fluxes predicted by the model lacking occlusive feedbacks would lead to differences in oxygenation in the trunk tissues. To do this, we modeled oxygen diffusion through the trunk by a reaction-diffusion equation, using the formulation and oxygen consumption coefficients derived by [40], and treating the vessels as oxygen sources (Fig. 1D, and see Supplementary Materials for details of the model). Note that our model includes only the contribution of oxygen perfusion from the blood to trunk oxygenation. For a real zebrafish at 4 dpf, these uneven oxygen levels would be compensated for by diffusion through the skin. However, our model shows that diffusion within the zebrafish trunk could not compensate even at 4 dpf for uneven perfusion, and since the topology of the trunk network does not change during embryogenesis, we would expect differences in oxygen levels to eventually disadvantage the embryo.

C. In real zebrafish, red blood cells are uniformly distributed among trunk vessels

In contrast with the resistor network model, which predicts that the first Se vessel short circuits the network, measured RBC fluxes are nearly uniform between Se-vessels in living zebrafish. We tracked fluorescently tagged red blood cells moving through each of the 12 SeAs within a living, sedated, zebrafish (see Methods), over a total time interval of 38s per SeA. Fluxes in individual vessels varied greatly in time, due to the rapid change of blood pressures within the DA, over the zebrafish cardiac cycle [28], so the variability of flows rates was large for each vessel. However,

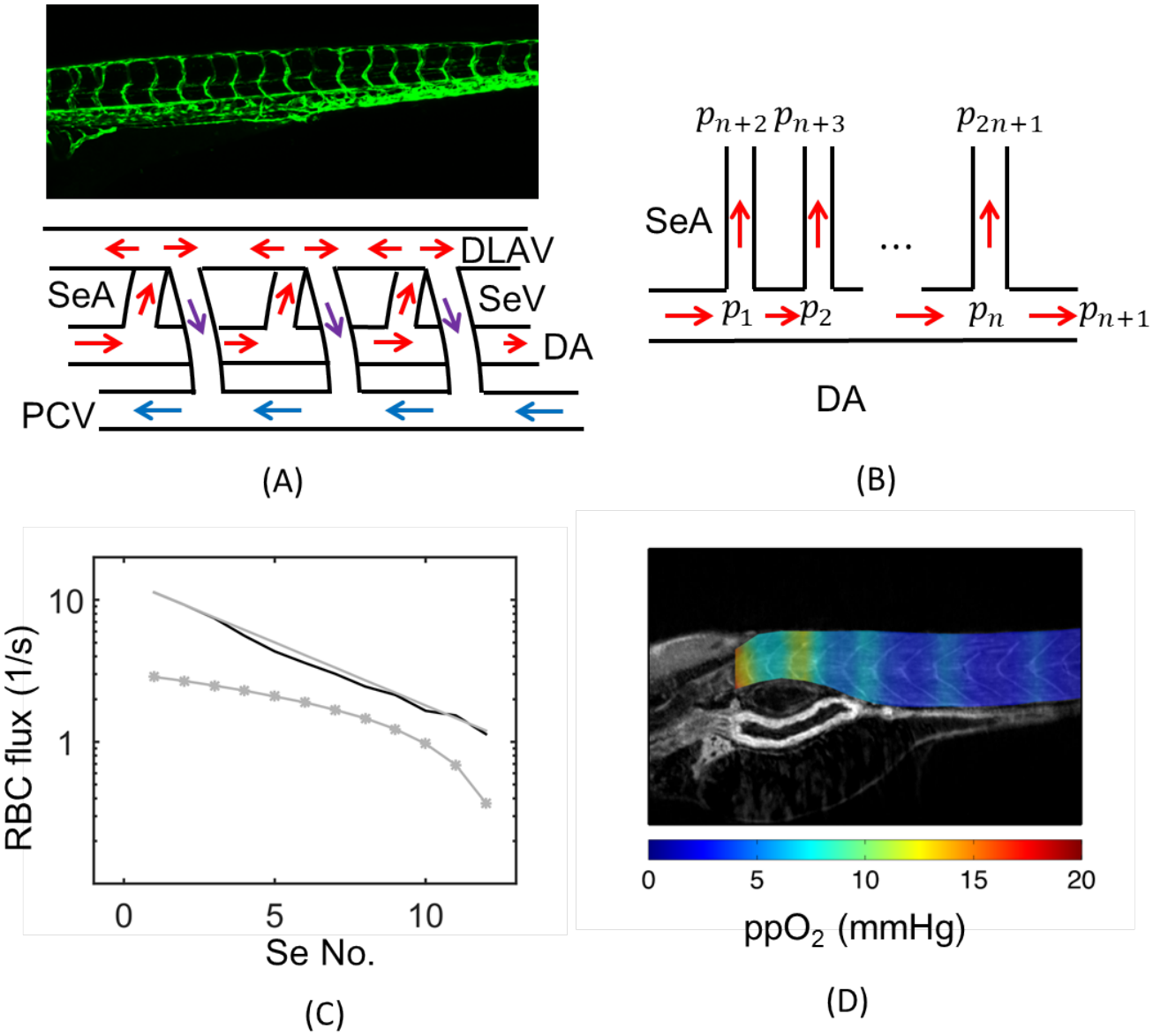

FIG. 1. The embryonic zebrafish trunk is perfused by a series of parallel intersegmental arteries (SeAs). Hydraulic models for the network predict that the first of these SeA will short circuit flow through the trunk. (A) 3 day post-fertilization zebrafish embryo trunk network and wiring diagram showing PCV, DA and Se vessels. A third trunk vessel, the dorsal longitudinal anastomotic vessel (DLAV), passes along the symmetry plane of the trunk. We do not include the DLAV in our analysis. (B) Representation of the same network as a set of hydraulic resistors. (C) The resistor network model predicts that cell fluxes decrease exponentially with distance from the heart (Black curve: numerical solution using real geometric parameters, Gray line: asymptotic model. For these two curves flow rates are multiplied by the concentration of red blood cell $\rho = 0.003\ \mu m^{-3}$ measured in [35]). By contrast an occlusive feedback model incorporating uniform occlusion strength $\alpha_c = 1.01 \times 10^{-6} g/\mu m^4 s$ did not lead to more uniform distribution of red blood cell fluxes between vessels (Gray stars). (D) Anisotropic fluxes produce uneven oxygen perfusion within the trunk. Zebrafish CT image reproduced from[41]

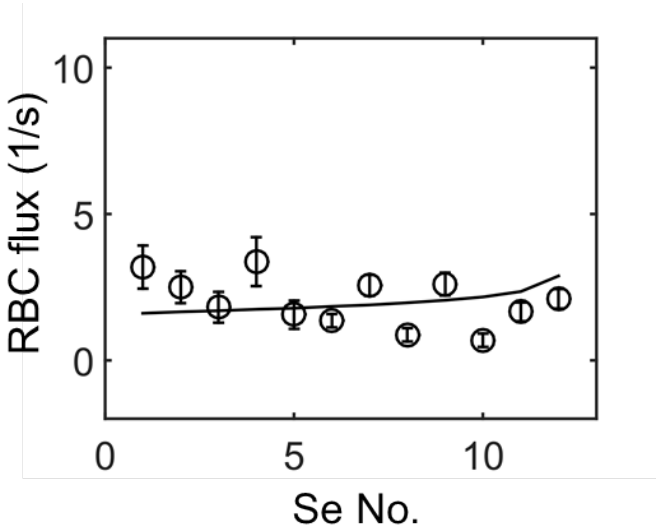

FIG. 2. Measured cell fluxes in real zebrafish embryos are almost uniform across all microvessels. Bars: 95% confidence interval on flux. Black: A model incorporating tuned occlusion strength agrees well with the data, see Result Section.

mean fluxes varied little between different vessels mean fluxes varied little from vessel to vessel (Fig. 2). When flow rates were correlated against the index of SeA (denoting the SeA closest to the heart as $i = 1$, and the furthest SeA as $i = 12$), the fitted change in flux moving from one vessel to the next was: $m = -0.115 \pm 0.003\ 1/s$ (mean $\pm$ standard deviation), so that there was no signature of the predicted experimental decay.

D. In real zebrafish, red blood cells fluxes show occlusive feedbacks, with variable strengths

There are two major ingredients missing from the hydraulic resistor network model that could explain the anomalies between the predictions of that model and the real zebrafish flow rate data: skimming of red blood cells and occlusive feedbacks effects [32, 42]. Skimming occurs because red blood cells do not divide in the same ratios as whole blood when blood vessels branch. When a red blood cell passes through a junction at which a vessel branches into two daughter vessels of different sizes, it is more likely to enter the larger daughter vessel than would be expected based on the ratio of fluxes in the two daughter vessels. Phase skimming can not explain the uniform distribution of red blood cells seen across real zebrafish microvessels: to correct for an 11-fold difference in flow rates between first and last Se vessels, there would need to be an 11-fold increase in hematocrit between these vessels. This was not observed in our experiments. Indeed, [29] explicitly fit measurements of red blood cell fluxes at the branch points of blood vessels, and parameterized the amount of phase skimming that occurred. When we applied this model to the zebrafish

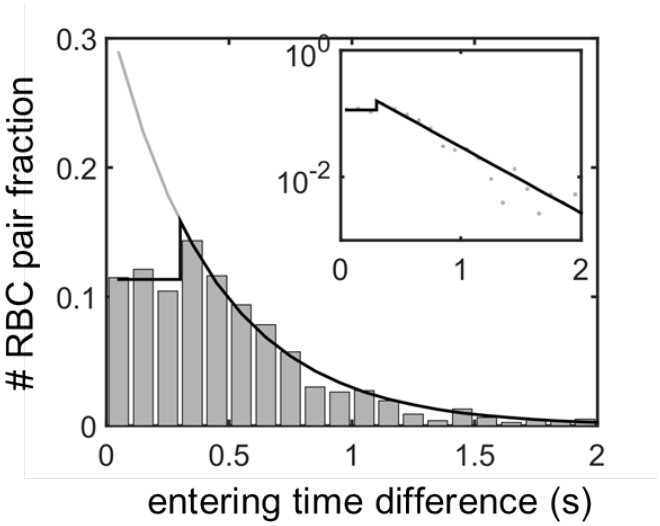

FIG. 3. Red flood cell flows in the real intersegmental artery network are affected by feedbacks, as shown by a significantly lower fraction of red blood cells entering the same vessel within 0.3s of each other. Shown: Distribution of inter-entry times for cells entering all 12 SeAs. In the absence of feedbacks, inter-entry times will be exponentially distributed (black curve), while real inter-entry times follow an exponential distribution only when cells enter the vessel more than 0.3s apart, and have uniform distribution when cells enter the vessel within 0.3s of each other (black star curve). Inset: The semi-log plot of the linear-exponential distribution (black curve) fits well to the data (gray dots) above 0.3s, showing the exponential distribution when the inter-entry time is long enough for the first cell to leave the vessel. We bin the inter-entry time intervals into $0.1s$ bins which is the typical time resolution of our videos.

microvasculature, only minute variations in hematocrit were predicted between different SeAs (see Supplementary Materials).

By contrast, we observed large feedback effects within the SeA. Using our red blood cell tracking data, we plotted the inter-entry intervals, i.e. the times between consecutive red blood cells entering each vessel, condensing data from all SeAs since all vessels have the same approximate rate of blood cell entry (see Fig. 3). In the absence of feedbacks, we would expect the inter-entry times to be distributed randomly, i.e. as an exponential random variable. Our red blood cell tracking shows that a single red blood cell passes through an SeA in a mean time of 0.3s. Inter-cell entry intervals larger than 0.3s (i.e. cell entries into unoccupied SeAs) were distributed exponentially (see the inset to Fig. 3). However, inter-entry intervals less than 0.3s were not exponentially distributed, and we saw far fewer cells entering vessels less than 0.3s apart (i.e. while the vessels were already occupied by other cells) than would be expected based on the exponential distribution (Fig. 3, main panel). In fact we found that inter-entry intervals less than 0.3s were approximately uniformly distributed. These observations are suggestive of a negative feedback mechanism, whereby

entry of a red blood cell into an SeA reduces for some time afterward the probability of another red blood cell entering the same SeA.

We tested for statistical support for the presence of negative feedback by two methods. First, we extrapolated the exponential fit for time intervals greater than 0.3s to estimate the number of cells that should enter the SeA between 0 and 0.3s, if cell entries into SeA were independent events. For the zebrafish trunk data this amounted to 533 cell entries, compared to the 261 actually observed, and the difference in statistically significant by the Fisher's exact test ($p = 3.9 \times 10^{-22}$ against independence). Secondly, we fit the distribution of cell entry times directly, to compare an independent model with an exponential probability density function (pdf), with a model in which the feedbacks were modeled by a composite pdf, with uniform probabilities for inter-cell entry intervals less than 0.3s, and an exponential pdf for cell entry intervals greater than 0.3s. The Akaike Information Criterion score corrected for small samples (AICc) [43] for the composite pdf was 4.02×10^3, whereas the AICc for the pdf assuming independence was 4.07×10^3, supporting the inclusion of feedback effects.

In mammals red blood cells must squeeze through narrow capillaries. Passage through these narrow vessels is facilitated by specific cellular adaptations – cells are un-nucleated, and have a biconcave shape, assisting cell deformation. By contrast zebrafish red blood cells are almost spherical and are nucleated. However, since the diameters of SeAs are closely comparable to red blood cell diameters (both $6\,\mu$m), we speculated that zebrafish red blood cells may also fit tightly within the SeAs. We directly measured these dynamics by measuring the dependence of the velocity within a SeA upon the number of red blood cells contained in the vessel (see Methods). Velocities within each SeA are affected by the phase of the cardiac cycle, so there is large variability in these velocities, and pressures are also affected by changes in conductivity throughout the network (Fig. 4A). However, in each vessel we found that $1/v$ increased linearly with the number of cells, n, consistent with the model for occlusion in Equation (1). In physical terms, when a cell travels through a vessel, it almost blocks the vessel. Because a large pressure difference must be maintained over the cell to push it forward through the SeA, flow within the vessel slows, so that fewer red blood cells enter a vessel once it contains a cell.

We measured the occlusive effect within each SeA, i.e. the parameter α_c in Equation (1) by fitting the slope of the graph of $1/v$ against n (see Fig. 4A). The intercept of the graph is given by the speed within the SeA when it contains no red blood cells. We get that speed from a model of flow without occlusive feedbacks, described above, so there is only one free parameter to be estimated for each SeA. Equation (1) represents a form of the Fahraeus-Lindqvist effect, since it gives that the resistance of each vessel increases as hematocrit increases. The parameter α_c represents

the resistance per cell, and it depends on the relative size of the cell and SeA (i.e. how tightly the red blood cell must be squeezed to travel along the vessel), as well as upon the surface chemistry of both. In particular, [30] built a physically informed model of cells moving through a narrow vessel, including both cell deformation, and interactions between the cell and the vessel glycocalyx: a polymer brush that covers and lubricates the endothelial lining of the vessel. They found that α_c is highly sensitive to biophysical parameters: the thickness of the glycocalyx layer as well as its porosity (i.e. to the concentration of polymer), as well as to small changes in vessel radius. Using values for these parameters consistent with experiments in the model (mammalian) vessels studied by [30], predicted values of α_c varied over two orders of magnitude.

Because of the potential for controllability for the occlusive effect, α_c, we measured α_c independently in each of the twelve SeAs, in all cases by fitting the data for the dependence of $1/v$ upon n (see Supplementary Materials for more details of the fit). The experimentally measured occlusion strength decreased from first to last SeA (Fig. 4B), over a range of $\alpha_c = 3.0 \times 10^{-7} \sim 2.8 \times 10^{-5}\ g/\mu m^4 s$. In physical terms, red blood cells occlude. These values are consistent with the range given in Secomb et al.'s model [30] in which α_c could range from $\alpha_c = 1.8 \times 10^{-7}$ to $1.6 \times 10^{-5}\ \ g/\mu m^4 s$. Note however, that the micromechanical model of [30] was created for mammalian red blood cells in capillaries, and that glycocalyx parameters have not been measured in zebrafish.

E. Uniformizing red blood distributions requires tuning occlusive effects between different micro-vessels

We simulated around 17 min of red blood cell flow through the zebrafish vascular network, assuming the same occlusive effect for every microvessel, using a discrete model in which every red blood cell trajectory was tracked and in which vessel resistances were modeled using Equation (1) (see Materials and Methods). The model continued to predict that red blood cell fluxes within vessels decrease exponentially with distance from the heart (Fig. 1C). This can be rationalized as follows: If α_c is identical between intersegmental vessels, and phase skimming is assumed to be negligible, then the model predicts that the resistance of eac h vessel will increase on average from the value given by the Hagen-Poiseuille law by $\alpha_c \cdot \mathrm{Hct} \cdot V/V_c$, where V is the volume of the vessel, V_c is the volume of a single cell and Hct is the hematocrit. We have already demonstrated in the approximate model derived in Section III B that variation in SeA length from head to tail of the zebrafish contribute very little to partitioning of red blood cell fluxes between SeAs, so changing the resistance of each vessel by an amount simply proportional to its length, will similarly not affect the exponential decay of red blood cell fluxes.

The potential effect size from including occlusive feedbacks is much larger than the effect of phase skimming:

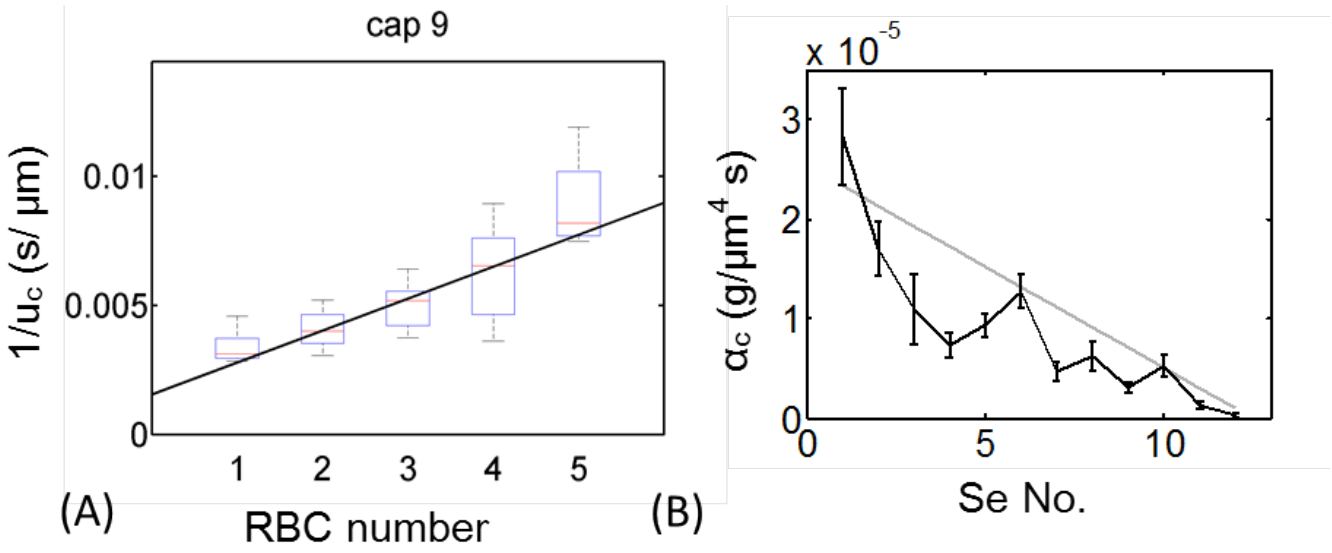

FIG. 4. Occlusion of SeAs by cells feeds back onto the flow through the SeA. (A) Equation 1 predicts that the reciprocal of cell velocity increases linearly with the number of cells in each Se vessel. Displayed: data from the 9th Se vessel (Boxplot) and regression to determine feedback per cell, α_c (curve). The y-intercept is determined from the theoretical plasma velocity in a network with no cells. For data on other Se vessels see Supplementary Materials. (B) Measured α_c values decrease from first to last Se vessel. Gray line: linear regression of α_c against Se vessel index. Bars: 95% confidence intervals calculated by bootstrapping.

predicted flow rates decreased by a factor of more than 7 compared to the values predicted by the hydraulic resistor network model. We therefore hypothesized that varying occlusive effects between different SeAs may uniformly distribute red blood cells through the network. To probe how variations in occlusive feedback could be used to control the distribution of red blood cells, we studied a reduced model of the vascular network. Specifically, we built a mean field model for the flows in a model network including only the first and last SeAs, as well as the direct connection between the DA and PCVs (the labeling of vessels and branching points is shown in Fig. 5A). In each vessel the cells were assumed to be well-mixed and cell fluxes are divided in proportion to flow rates at all nodes. Then the hematocrit will be the same in all vessels. For simplicity we express our equations in terms of the concentration of red blood cells (# / volume), ρ, rather than the hematocrit. ρ and hematocrit are simply related by $\rho = \mathrm{Hct}/V_c$. Let R_i be the modified resistance of the ith vessel according to Equation (1). Then by applying Kirchoff's first law at the branching points at which first and second Se vessel branch off from the aorta, we obtain the pressures at these

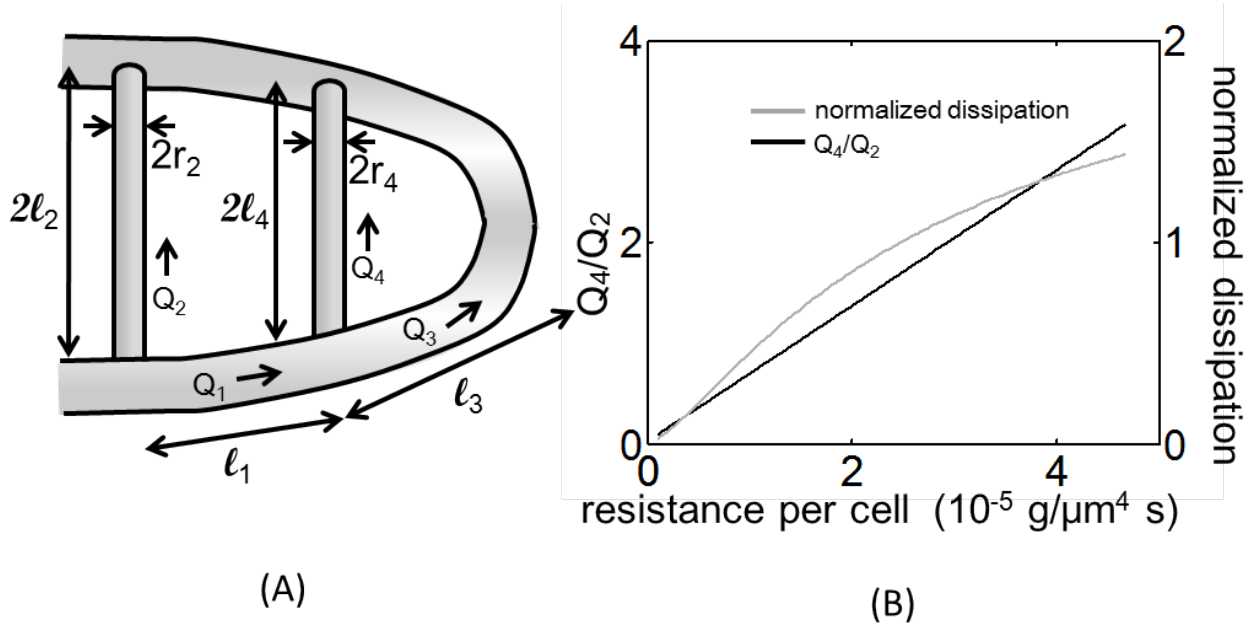

FIG. 5. A reduced vascular network model shows that occlusive effects need to be varied between SeAs, and exposes trade-offs between flow uniformity and transport efficiency. (A) Diagram of the reduced model of the network showing vessel lengths l_i, fluxes Q_i, and radii r_i. (B) Increasing the occlusion strength α_2 increases flux uniformity, measured by the ratio of fluxes in the last and the first Se (black curve), but also increases dissipation (gray curve), if the total flux through both Se vessels is maintained.

points, i.e. p_1 and p_2:

$$F = \frac{p_1 - p_2}{R_1} + \frac{p_1}{R_2}, \frac{p_1 - p_2}{R_1} = \frac{p_2}{R_3} + \frac{p_2}{R_4}, \tag{4}$$

Here F is the total flux of blood into the network, and we can solve Eqns. (4) by linear algebra (see Supplementary Materials). Of particular interest is is the ratio of fluxes in the two Se, which measures how uniformly the different vessels are kept supplied with cells:

$$\frac{Q_4}{Q_2} = \frac{R_{2_0} + V_2\rho\alpha_2}{R_{4_0} + V_4\rho\alpha_4}\left(1 + \frac{R_1}{R_3} + \frac{R_1}{R_4 + V_4\rho\alpha_4}\right)^{-1} \tag{5}$$

Here α_2, α_4 are respectively the values of α_c in the first and last SeA, R_{2_0}, R_{4_0} are the resistances of the two SeAs in the absence of red blood cell occlusion, and V_i is the volume of vessel i. Many of the parameters in Eq.(5) are tightly constrained: the dimensions of the two Se vessels are similar (in fact $R_{2_0} \approx 2R_{4_0}$ and $V_2 \approx 2V_4$), moreover, since the vessel network extends during development and supplies the tail fin in adult zebrafish[44], the aorta must maintain the same radius along its length, leading to $R_1 \approx 11R_3$. Thus the second factor of Eqn. (5) $\left(1 + \frac{R_1}{R_3} + \frac{R_1}{R_4 + V_4\rho\alpha_4}\right)^{-1}$ has

an upper bound $\frac{1}{12}$. Therefore the only parameters that can be used to increase Q_4/Q_2 (i.e. eliminate short-circuiting of the network by the first SeA) are the relative sizes of α_2 and α_4. Q_4/Q_2 is largest if $\alpha_2 \gg \alpha_4$, i.e. if occlusion effects are stronger in the first SeA. Thus uniformization of flow requires stronger occlusion in vessels close to the heart, consistent with experimental observations in real zebrafish (Fig. 4B).

However our reduced model also shows that varying occlusion strengths between vessels creates trade-offs between uniformity and the transport efficiency, measured by the dissipation:

$$D_{\text{network}} = \frac{8\mu_{wb}}{\pi r_a^4}(\ell_1 Q_1^2 + \ell_3 Q_3^2) + \frac{8\mu_{pl}}{\pi r_c^4}(\ell_2 Q_2^2 + \ell_4 Q_4^2) + \rho(Q_2^2 V_2 \alpha_2 + Q_4^2 V_4 \alpha_4). \quad (6)$$

(See Supplementary Materials for derivation). Here ℓ_i is the length of the ith vessel, r_a is the radius of the DA, and r_c is the radius of the Se vessels. To compare equivalent networks as we vary α_2 we also vary F to keep the total flux through the pair of Se vessels ($Q_2 + Q_4$) constant. Dissipation in the thin layers of fluid forced through the Se vessel around each RBC dominates D_{network}, so as α_2 increases D_{network} increases. The highest ratios of Q_4/Q_2 are therefore also the most dissipative networks (Fig. 5B).

F. Observed variation in occlusive effects optimizes uniform distribution of red blood cells

We modified our simulation from Section III E, to incorporate the observed variations in occlusive effects; i.e. using the different measured values of α_c in each vessel. When vessels were assigned the experimentally measured values of α_c, red blood cells became uniformly distributed between SeAs, and matched closely to the real flow observations (see Figure 2).

Are measured variations in occlusive effects really represented adaptive tuning of the zebrafish cardiovascular network, rather than incidental changes caused by aging? New SeAs are progressively added to the trunk at the tail of the zebrafish as the trunk elongates, and we wanted to evaluate the alternate hypothesis that the younger vessels farther from the heart had lower occlusive effects simply because they have a thinner glycocalyx coating, or else because structural adaptation of vessels to the flows through them may tend to reduce vessel radii over time [45]. Although neither alternate explanation can be totally ruled out, we were able test how close the observed distribution of occlusive effects is to one that optimizes the uniform partitioning of red blood cell flows between vessels. Specifically, we ran discrete cell simulations of flow within the network for different distributions of occlusive effects: that is we varied $\Delta\alpha_c$, which is the difference in α_c between the first and last SeAs, assuming a linear variation of α_c in the intermediate vessels. For each model network, we calculated the coefficient of variation (CV) in the red blood cell

flux, i.e. the standard deviation in red blood cell flow rate over all vessels, normalized by the mean flow rate. Smaller values of CV correspond to a more uniform distribution of red blood cell flows. Using discrete cell simulations, i.e. tracking every cell trajectory, produces more accurate estimates of red blood cell fluxes in principle than the continuum modeling from Section III E, because cell number fluctuations within each SeA are comparable to the mean number of cells. Since the change in resistance of a vessel depends on the number of cells in the vessel according to Equation (1), the distribution of red blood cell flows for a given variation in occlusive effects depends on hematocrit. Accordingly, we varied both hematocrit and occlusive effect variation independently in our simulations. We found for any fixed hematocrit, near uniform flux (CV close to 0) can be achieved only over a narrow range of occlusive effect variations (Fig. 6A). Too little variation, and the first SeA short-circuits the network, as discussed in Sections III B and III E. But too much variation in occlusive effects can have the opposite effect, leading to the vessels furthest from the heart receiving more flow than vessels closest to the heart. The optimal variation in the occlusive effects depends on the hematocrit producing a curve in $(\Delta\alpha_c, \rho)$ space. We found that the observed occlusion effect strength is close to the optimal value for the real zebrafish hematocrit[35] (Fig. 6A).

IV. DISCUSSION

Our work shows that feedbacks associated with the occlusion of fine vessels by the red blood cells that pass through may carry previously unreported adaptive benefits for control of blood flows within the microvasculature. Although our experimental observations and modeling are focused on zebrafish, which are a model for vascular development, it is likely that similar feedbacks are significant within mammalian microcirculatory systems, where the deformation of cells to pass through capillaries is, if anything, even more extreme than in the zebrafish. Note, however, the discoidal shape of mammalian red blood cells enables them to organize into trains of tightly packed cells or rouleaux [46]. Since many red blood cells may pass through a single capillary in quick succession as rouleaux, the organization of the mammalian vascular network allows for both positive and negative feedbacks.

Capillary networks have been hypothesized to be organized to minimize the cost of blood transport [18, 20]. Although large vessels seem to conform very closely to this organizing principle [20, 21], the tuning of occlusive effects to uniformly distribute red blood cell flows takes the zebrafish vascular network far from the configuration that minimizes transport costs. In particular, at the physiological hematocrit, if the same (smallest) occlusive effect, α_c, is assigned to each vessel then the dissipation in the network could be reduced by a factor of 11 (Fig. 6B). At the same time, more uniform partitioning of cell fluxes between different SeAs (i.e. a lower value of the Coefficient of

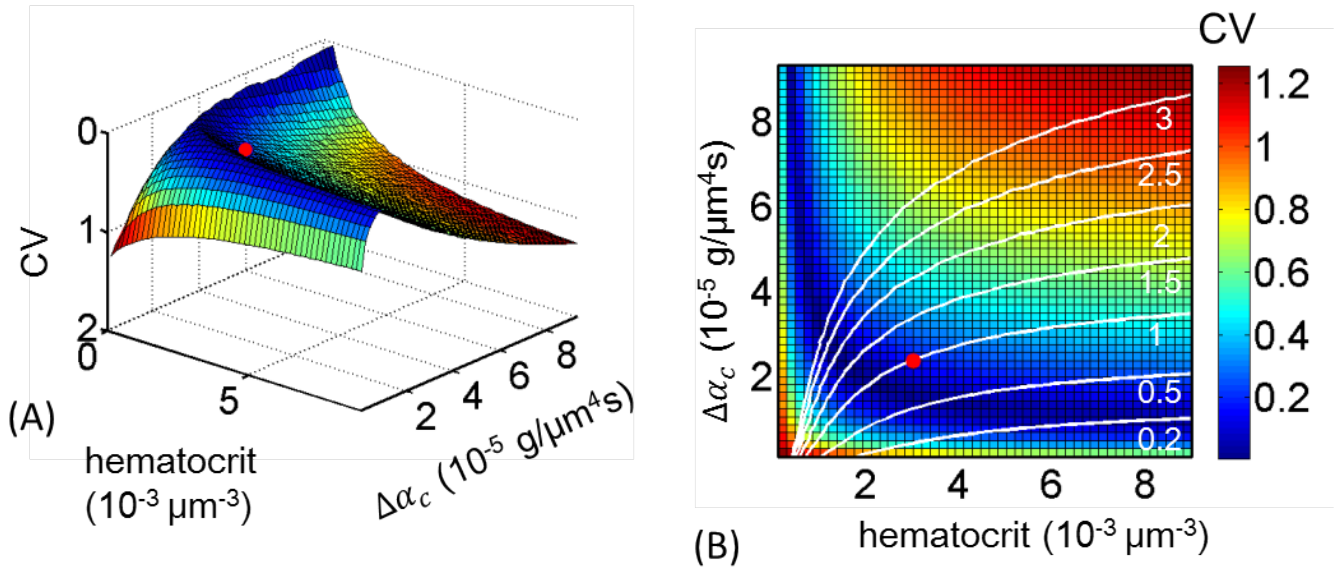

FIG. 6. Tuned occlusion strengths uniformly distribute flow across different Se vessels. (A) Dependence of flux uniformity upon controllable parameters is explored by allowing blood cell concentration, ρ, and difference in occlusive effects between first and last Se vessel, $\Delta\alpha_c$, to vary independently and computing the coefficient of variation (CV) for flow through all Se vessels. Flux uniformity is achieved only within a narrow manifold of values of blood cell concentrations and occlusive effect differences. The empirical values (red dot) lie close to this optimal manifold. (B) Higher uniformity can be achieved if blood cell concentration is decreased (moving leftward from the red dot) but at the cost of increasing dissipation. Transport costs are reduced if $\Delta\alpha_c$ is decreased (moving downward), and can be reduced by 11-fold if there is no occlusive effect variation in the cost of reducing uniformity of RBC fluxes. Colors show CV values from (A) and white curves show level sets of dissipation; the dissipation is normalized by its value in the real zebrafish.

Variation of red blood cell flow rates) is possible but altering physiological parameters further decreases the transport efficiency. For example decreasing blood cell concentration, ρ, increases uniformity of flux, but at the cost of increasing dissipation if the total cell supply to all Se vessels is to kept fixed (Fig. 6B).

The ability of SeAs to vary the occlusive effect α_c over three orders of magnitude is consistent with previous modeling of red blood cell and microvessel mechanics, and endows the network with tremendous control over red blood cell flow rates. It is natural to ask whether and how uniform red blood cell flux partitioning can be maintained against the numerous sources of perturbation that occur in real cardiovascular networks. In real organisms, microvascular networks may be disrupted by trauma, micro-anneurysms, or by systemic conditions like diabetes mellitus [47]. As a first step toward answering this question, we considered the effect of well-characterized natural variability in SeA

spacing [48], and of the notch mutation which alters connectivity [49] upon the ability of the trunk network to uniformly distribute red blood cell fluxes. We found that under a wide range of vessel spacing variability, red blood cell fluxes remained uniform across all SeAs (see Supplementary Materials). Indeed vessel spacing variability has no detectable effect on zebrafish growth and maturation. By contrast, in notch mutant zebrafish the cardiovascular network is malformed, with a shunt connection forming between aorta and principal cardinal vein. Since the diameter of the shunt is much larger than the cell diameter, there is negligible occlusive feedback within the shunt, causing it to irreparably short-circuit the vascular network. Shunt formation is lethal in embryos, and our model shows that it creates conditions under which uniform perfusion of the trunk is impossible.

Although we are able to directly demonstrate that occlusive feedbacks vary between different the SeAs, and this variation is consistent with optimization of feedback strengths to ensure uniform distribution of red blood cells across trunk vessels, our model does not show what physical changes within vessels are used with the zebrafish network to modulate the occlusive effect. In our experiments we can not visualize the glycocalyx lining of the SeAs, and in fact we are aware of no previous works in which glycocalyx was measured in blood vessels simultaneously with flow. However, previous studies have reported large variations in glycocalyx porosity and thickness between different vessels [28, 50]. Alternatively, since cells must squeeze into SeAs, variations in vessel radius below the resolution limit of our microscopy method could also account for the variation in occlusive effect. The analysis is also silent on the mechanisms for coordinating occlusive effects across the network. Recent works have dissected structural adaptations in microvascular networks [45], as well as in biological transport networks generally [51]. These works have focused on the question of how a set of vascular elements that have information only about their own flows can alter their resistances in response to these cues to minimize dissipation within the network. This question is directly relevant to other objective functions – can vessels adapt their occlusive effects to the their flow to achieve uniform red blood cell transport?

The use of tuned occlusive effects creates uniform distribution of red blood cell fluxes through the zebrafish vascular network, but at the cost of increasing transport costs. Indeed if the network simply used the same value of α_c in every SeA we found that an 11 fold decrease in transport costs would be possible within the zebrafish trunk vasculature (Fig. 6B). Physically feedbacks from occlusion represent a form of congestion, and efficient transport networks, both natural [52] and artificial [10], are often organized to avoid congestion. Previous works have provided algorithms for constructing minimally dissipative networks given a prescribed set of sources and sinks [18, 19]. Our work suggests that other optimizing principles may govern microvascular network organization. Extending network optimization

algorithms to include flow uniformity is likely to further reveal the tradeoffs between uniformity and efficiency.

V. ACKNOWLEDGMENTS

This research was funded by grants from NSF (under grant DMS-1312543) and by a research fellowship from the Alfred P. Sloan Foundation. MR. SSC was also supported by the National Institutes of Health, under a Ruth L. Kirschstein National Research Service Award (T32-GM008185). The contents of this paper are solely the responsibility of the authors and do not necessarily represent the official views of the NIH. We thank the Taiwan Zebrafish Core Facilities at Academia Sinica (TZCAS) and at NHRI (TZCF) for providing Tg(gata1:dsRed; fli1a:EGFP) transgenic fish, and Jérémy Lévéque for performing early calculations for Figure 1C.

[1] G. Tomaiuolo, Biomicrofluidics **8**, 051501 (2014).

[2] G. B. West, J. H. Brown, and B. J. Enquist, Science **276**, 122 (1997).

[3] J. E. Hall, *Guyton and Hall textbook of medical physiology* (Elsevier Health Sciences, 2015).

[4] T. Savin, M. Bandi, and L. Mahadevan, Soft matter **12**, 562 (2016).

[5] T. Betz, M. Lenz, J.-F. Joanny, and C. Sykes, Proceedings of the National Academy of Sciences **106**, 15320 (2009).

[6] Y. Park, C. A. Best, T. Auth, N. S. Gov, S. A. Safran, G. Popescu, S. Suresh, and M. S. Feld, Proceedings of the National Academy of Sciences **107**, 1289 (2010).

[7] J. Wan, W. D. Ristenpart, and H. A. Stone, Proceedings of the National Academy of Sciences **105**, 16432 (2008).

[8] C. Hawkey, P. Bennett, S. Gascoyne, M. Hart, and J. Kirkwood, British journal of haematology **77**, 392 (1991).

[9] T. W. Secomb and R. Hsu, Biophysical journal **71**, 1095 (1996).

[10] D.-M. Chiu and R. Jain, Computer Networks and ISDN systems **17**, 1 (1989); H. Yang and M. G. H. Bell, Transport Reviews **18**, 257 (1998).

[11] S. Rao, Š. Bálint, B. Cossins, V. Guallar, and D. Petrov, Biophysical journal **96**, 209 (2009).

[12] C.-H. Wang and A. S. Popel, Mathematical biosciences **116**, 89 (1993).

[13] D. Kleinfeld, P. P. Mitra, F. Helmchen, and W. Denk, P. Natl. Acad. Sci. USA **95**, 15741 (1998).

[14] E. Chaigneau, M. Oheim, E. Audinat, and S. Charpak, P. Natl. Acad. Sci. USA **100**, 13081 (2003).

[15] T. Schwerte, D. Überbacher, and B. Pelster, J. Exp. Biol. **206**, 1299 (2003).

[16] T. J. Chico, P. W. Ingham, and D. C. Crossman, Trends in cardiovascular medicine **18**, 150 (2008).

[17] J. R. Banavar, F. Colaiori, A. Flammini, A. Maritan, and A. Rinaldo, Physical Review Letters **84**, 4745 (2000).

[18] S. Bohn and M. O. Magnasco, Physical review letters **98**, 088702 (2007); C. D. Murray, P. Natl. Acad. Sci. USA **12**, 207 (1926).

[19] E. Katifori, G. J. Szöllősi, and M. O. Magnasco, Phys. Rev. Lett. **104**, 048704 (2010).

[20] T. F. Sherman, The Journal of general physiology **78**, 431 (1981).

[21] M. Zamir, P. Sinclair, and T. H. Wonnacott, Journal of biomechanics **25**, 1303 (1992).

[22] J. Schindelin, I. Arganda-Carreras, E. Frise, V. Kaynig, M. Longair, T. Pietzsch, S. Preibisch, C. Rueden, S. Saalfeld, B. Schmid, *et al.*, Nature methods **9**, 676 (2012).

[23] J. R. Hove, R. W. Köster, A. S. Forouhar, G. Acevedo-Bolton, S. E. Fraser, and M. Gharib, Nature **421**, 172 (2003).

[24] E. A. Jones, F. le Noble, and A. Eichmann, Physiology **21**, 388 (2006).

[25] T. J. Pedley, Journal of engineering mathematics **47**, 419 (2003).

[26] U. Windberger, A. Bartholovitsch, R. Plasenzotti, K. Korak, and G. Heinze, Exp. Physiol. **88**, 431 (2003).

[27] J. Lighthill, *Mathematical biofluiddynamics*, Vol. 17 (Siam, 1975).

[28] M. H. Malone, N. Sciaky, L. Stalheim, K. M. Hahn, E. Linney, and G. L. Johnson, BMC biotechnology **7**, 40 (2007); S. Weinbaum, J. M. Tarbell, and E. R. Damiano, Annu. Rev. Biomed. Eng. **9**, 121 (2007).

[29] A. R. Pries and T. W. Secomb, American Journal of Physiology-Heart and Circulatory Physiology **289**, H2657 (2005).

[30] T. Secomb, R. Hsu, and A. Pries, American Journal of Physiology-Heart and Circulatory Physiology **274**, H1016 (1998).

[31] M. Schindler and A. Ajdari, Phys. Rev. Lett. **100**, 044501 (2008).

[32] A. Pries, K. Ley, M. Claassen, and P. Gaehtgens, Microvascular research **38**, 81 (1989).

[33] A. Krogh, *The anatomy and physiology of capillaries*, Vol. 18 (Yale University Press, 1922).

[34] B. W. Zweifach and H. H. Lipowsky, Circ. Res. **41**, 380 (1977).

[35] J. M. Murtha, W. Qi, and E. T. Keller, Comparative Med. **53**, 37 (2003).

[36] P. Vennemann, K. T. Kiger, R. Lindken, B. C. Groenendijk, S. Stekelenburg-de Vos, T. L. ten Hagen, N. T. Ursem, R. E. Poelmann, J. Westerweel, and B. P. Hierck, Journal of biomechanics **39**, 1191 (2006).

[37] B. Pelster and W. W. Burggren, Circ. Res. **79**, 358 (1996).

[38] P. Rombough and H. Drader, J. Exp. Biol. **212**, 778 (2009).

[39] B. M. Weinstein, D. L. Stemple, W. Driever, and M. C. Fishman, Nat. Med. **1**, 1143 (1995).

[40] S. Kranenbarg, J. G. van den Boogaart, and J. L. van Leeuwen, Anim. Biol. **53**, 339 (2003).

[41] D. Salgado, C. Marcelle, P. D. Currie, and R. J. Bryson-Richardson, Dev. Biol. **372**, 1 (2012).

[42] A. Pries, T. Secomb, P. Gaehtgens, and J. Gross, Circulation research **67**, 826 (1990).

[43] C. M. Hurvich, J. S. Simonoff, and C.-L. Tsai, Journal of the Royal Statistical Society: Series B (Statistical Methodology) **60**, 271 (1998).

[44] D. M. Parichy, M. R. Elizondo, M. G. Mills, T. N. Gordon, and R. E. Engeszer, Dev. Dynam. **238**, 2975 (2009); P. E. Bayliss, K. L. Bellavance, G. G. Whitehead, J. M. Abrams, S. Aegerter, H. S. Robbins, D. B. Cowan, M. T. Keating, T. O'Reilly, J. M. Wood, *et al.*, Nat. Chem. Biol. **2**, 265 (2006).

[45] A. Pries, T. Secomb, and P. Gaehtgens, American Journal of Physiology-Heart and Circulatory Physiology **275**, H349 (1998).

[46] S. Chien and K.-M. Jan, Microvascular Research **5**, 155 (1973).

[47] V. Fonseca and A. Jawa, The American journal of cardiology **96**, 13 (2005); R. E. Pecoraro, G. E. Reiber, and E. M. Burgess, Diabetes care **13**, 513 (1990); P. Reichard, B.-Y. Nilsson, and U. Rosenqvist, New England Journal of Medicine **329**, 304 (1993); G. J. Biessels, S. Staekenborg, E. Brunner, C. Brayne, and P. Scheltens, The Lancet Neurology **5**, 64 (2006).

[48] S. Isogai, M. Horiguchi, and B. M. Weinstein, Dev. Biol. **230**, 278 (2001).

[49] N. D. Lawson, N. Scheer, V. N. Pham, C.-H. Kim, A. B. Chitnis, J. A. Campos-Ortega, and B. M. Weinstein, Development **128**, 3675 (2001).

[50] K. Haldenby, D. Chappell, C. Winlove, K. Parker, and J. Firth, Journal of vascular research **31**, 2 (1994).

[51] D. Hu and D. Cai, Phys. Rev. Lett. **111**, 138701 (2013); L. L. Heaton, E. López, P. K. Maini, M. D. Fricker, and N. S. Jones, Proceedings of the Royal Society of London B: Biological Sciences **277**, 3265 (2010); H. Ronellenfitsch and E. Katifori, arXiv preprint arXiv:1606.00331 (2016).

[52] P. C. Hickey, H. Dou, S. Foshe, and M. Roper, arXiv preprint arXiv:1601.06097 (2016).